Multigranular exocytosis of Weibel-Palade bodies in vascular endothelial cells

Karine M. Valentijn,[1] Linda F. van Driel,[1] Marjon J. Mourik,[1] Gert-Jan Hendriks,[1] Tom J. Arends,[1] Abraham J. Koster,[1] and Jack A. Valentijn[1]

[1]Department of Molecular Cell Biology, Section Electron Microscopy, Leiden University Medical Center, Leiden, The Netherlands

Regulated exocytosis of Weibel-Palade bodies (WPBs) is a pivotal mechanism via which vascular endothelial cells initiate repair in response to injury and inflammation. Several pathways have been proposed to enable differential release of bioactive molecules from WPBs under different pathophysiologic conditions. Due to the complexity, many aspects of WPB biogenesis and exocytosis are still poorly understood. Herein, we have investigated the regulated exocytosis of the major WPB constituent, von Willebrand Factor (VWF), which upon its release forms strings of up to several millimeters long that capture circulating platelets and thereby initiate the formation of a haemostatic plug. Using correlative, fluorescence, and electron microscopic imaging techniques, we provide evidence that multigranular exocytosis is an important pathway for VWF release in secretagogue-challenged human umbilical vein endothelial cells. A novel membrane-delimited structure (secretory pod) was identified as the site of WPB coalescence and VWF exocytosis. Clathrin-coated profiles present on the secretory pods suggested remodeling via compensatory membrane retrieval. Small, 30- to 40-nm cytoplasmic vesicles (nanovesicles) mediated the fusion of WPBs with secretory pods. Multigranular exocytosis may facilitate VWF string formation by pooling the content of multiple WPBs. In addition, it may provide a novel mechanism for the differential release of WPB cargo. (*Blood*. 2010;116(10):1807-1816)

Introduction

Regulated exocytosis from vascular endothelial cells forms the first line of repair following tissue damage and inflammation.[1] Endothelial-specific secretory granules, the so-called Weibel-Palade bodies (WPBs),[2] release their contents in response to various physiologic stimuli such as physical trauma, mediators of inflammation, and hypoxia. The major secretory product of WPBs, von Willebrand Factor (VWF), assembles into remarkably long strings (up to several millimeters long) that capture flowing platelets and bind to connective tissue at the site of vascular injury to form a hemostatic plug.[3-5] WPBs have a distinctive elongated shape of 0.1 to 0.2 μm wide and up to 5 μm long, with a uniform pattern of striations running along the longitudinal axis.[6-8] These striations represent VWF filaments that have assembled into helical tubules.[9] Packing of VWF multimers into tubules requires both the N-terminal domains of mature VWF and the cleaved VWF propeptide, while the maintenance of the tubules in WPBs depends on a pH-sensitive interaction between mature VWF and the propeptide.[4,10,11]

Microscopic imaging techniques have been instrumental in advancing our knowledge of WPB biogenesis and exocytosis. In particular, live-cell imaging studies using genetically labeled WPB cargo proteins have stressed the extraordinary plasticity of the regulated secretory pathway leading to WPB exocytosis.[12-16] Thus secretagogues that elevate intracellular cAMP levels cause a subset of WPBs to cluster at the level of the microtubule-organizing center so that they do not partake in exocytosis.[12] Secretagogues that elevate intracellular Ca^{2+} levels, on the other hand, do not elicit this effect. On the basis of these findings, and taking into account evidence for the existence of WPB subpopulations that except for VWF differ in their content of cargo molecules, it has been suggested that WPB clustering allows for the differential release of bioactive molecules from WPBs.[17] Further modulation of the release of WPB constituents is possible during the exocytosis process itself, as it has been shown that WPBs can engage in 2 modes of exocytosis, full-collapse and a slow form of kiss-and-run (lingering kiss).[14] In the latter mode, a 10- to 12-nm fusion pore is formed that acts as a molecular sieve allowing for the selective release of smaller molecules (interleukin-8, CD63) while larger molecules such as VWF are retained.

In the present report, we expand the palette of exocytosis modes of WPBs by providing evidence for multigranular exocytosis, that is, the homotypic fusion of secretory granules prior to exocytosis. Using confocal, live-cell, correlative, scanning electron, and electron tomographic imaging techniques applied to human umbilical vein endothelial cells (HUVECs), we identified a novel structure, which we termed secretory pod, and which represents a secretory intermediate resulting from the coalescence of WPBs. In addition, our data suggest that fusion of WPBs with secretory pods is mediated by tiny vesicles (nanovesicles). We propose that multigranular exocytosis of WPBs permits pooling of VWF to sustain the formation of VWF strings.

Methods

Cell culture

HUVECs, obtained from Lonza, were cultured as previously described.[6]

Submitted March 10, 2010; accepted April 29, 2010. Prepublished online as *Blood* First Edition paper, May 6, 2010; DOI 10.1182/blood-2010-03-274209.

The online version of this article contains a data supplement.

The publication costs of this article were defrayed in part by page charge payment. Therefore, and solely to indicate this fact, this article is hereby marked "advertisement" in accordance with 18 USC section 1734.

Regulated exocytosis of WPBs

Cells were preincubated in endothelial cell incubation medium (ECIM; 20mM HEPES, sodium salt, 112mM NaCl, 6mM KCl, 1mM magnesium sulfate, 1mM $CaCl_2$, 1.2mM K_2HPO_4, 5.6mM D-Glucose and 2% human serum albumin, pH 7.4) for 10 minutes at 37°C. Thereafter they were stimulated for 20 minutes with 80nM phorbol 12-myristate 13-acetate (PMA; Sigma-Aldrich; dissolved in DMSO; final DMSO concentration less than 0.01%). Control cells were incubated in parallel with vehicle only. Other secretagogues tested were thrombin (1 U/mL for 10 minutes; Sigma-Aldrich) and isoproterenol (1μM for 20 minutes; Sigma-Aldrich). Isoproterenol was administered in the presence of 100μM isobutylmethylxanthine (IBMX; Sigma-Aldrich). At the end of the stimulation, the incubation medium was removed and replaced with ice-cold fixative.

Immunofluorescence microscopy and live-cell imaging

For extracellular labeling of VWF, a sheep anti-VWF antibody conjugated to fluorescein isothiocyanate (FITC; Abcam) was added during the secretagogue stimulation at a dilution of 1:200 (50 μg/mL) unless indicated otherwise. Next, cells were fixed with 3% paraformaldehyde (PFA) in phosphate buffer for 30 minutes at 4°C and permeabilized for 5 minutes with 0.02% Triton-X100 in phosphate buffered saline (PBS), blocked in 5% normal goat serum (Dako) and labeled sequentially with primary and secondary antibodies. The cells were subsequently washed in PBS and the coverslips containing the cells were mounted on glass slides in Aqua-Polymount (Omnilabo). For correlative light and electron microscopy experiments, cells were counterstained with DAPI and kept in PBS during fluorescence microscopy. The primary antibodies used in this study were: FITC-conjugated sheep anti-VWF antibodies mentioned previously in this paragraph, rabbit anti-VWF antiserum from Dako, mouse monoclonal antibodies against the propeptide of VWF (CLB-Pro-14.3; generous gift from Dr J. Voorberg, Sanquin, Amsterdam), mouse monoclonal antibodies against CD63 from Abcam, and mouse monoclonal antibodies against Lamp-1 (mAb BB6; kindly provided by Dr S. Carlsson, Umeå, Sweden). The secondary antibodies were goat anti–rabbit or goat anti–mouse antibodies conjugated with Alexa-488, -568 or -594 fluorophores (Molecular Probes/Invitrogen). Imaging of the immunofluorescence was performed using a Leica SL or a Leica SP5 confocal laser-scanning microscope (Leica Microsystems). Image stacks as shown in Figure 1G were deconvolved and 3-dimensionally rendered using Huygens Pro sofware (SVI).

For live-cell imaging of VWF release, the culture medium was replaced by warm (37°C) ECIM. After allowing cells to equilibrate for 5 minutes, the ECIM was refreshed with ECIM containing PMA at a concentration of 80nM and FITC-conjugated anti-VWF antibodies at a dilution of 1:200. Images were recorded at 10-second intervals for up to 25 minutes using a Leica SP5 confocal laser-scanning microscope equipped with a temperature and humidity controlled stage. Time-lapse movies were generated using ImageJ (National Institutes of Health). The snapshots shown in Figure 2 were noise-filtered using ImageJ's "remove outliers" command with the threshold set to 10.

TEM and electron tomography

All procedures for transmission electron microscopy (TEM) and electron tomography were carried out as described previously.[6]

SEM

To prepare HUVECs for scanning electron microscopy (SEM), they were first fixed in 2% glutaraldehyde in 0.1M sodium cacodylate buffer (pH 7.4). Cells were then dehydrated in a graded ethanol series and critical point dried using a Baltec CPD-030 apparatus (Bal-tec). Coverslips containing the thus prepared cells were next mounted on SEM stubs and coated with a 6-nm layer of gold-palladium using a K650X sputter-coater (Emitech). The samples were viewed with a JEOL JSM-6700F field emission scanning electron microscope at 5.0 kV.

Correlative light and electron microscopy

For correlative light and TEM, HUVECs labeled with FITC-conjugated anti-VWF antibodies and DAPI were imaged with a Leica SP5 confocal microscope. Squares of the engraved grid in glass-bottom dishes (MatTek Corporation) were imaged at low magnification (10× objective) to obtain reference patterns of the DAPI nuclear stain. Thereafter, detailed images of the VWF label were made at higher magnification (63× objective) of cells in the same square. Following Epon embedding, squares of interest were trimmed and sections were collected on single-slot grids. Mosaic scans of the whole sections were made using software and Matlab scripts that have been developed in our laboratory. The stitched images were then analyzed in Imagescope (Aperio) where the nuclear patterns were used for matching with the fluorescence images. Correlated fluorescence and electron micrographs were scaled, flipped, rotated, and overlaid in Adobe Photoshop CS3.

For correlative light and SEM, gold EM finder grids (EMS/Aurion) were glued to the glass-bottom dishes prior to cell culture. The finder grids provided reference points that facilitated the retrieval of areas of interest in SEM mode. After fluorescence imaging, cells were fixed and processed for SEM as described in the previous section. Photoshop was used again to generate montages of fluorescence micrographs overlaid on SEM images.

Results

VWF is present in large spherical compartments

Secretagogue-challenged HUVECs displayed 3 distinct patterns of VWF-immunofluorescence that were absent in nonstimulated HUVECs: patches, dots, and filaments (supplemental Figure 1A, available on the *Blood* Web site; see the Supplemental Materials link at the top of the online article). It has previously been suggested that the irregularly shaped and reticular patches are located underneath the cells as a result of VWF secretion at the basal surface of the plasma membrane.[18] In agreement with this, we found that the patches were present in optical slices through the basal pole of the cells, while the dots and filaments came in focus at the apical pole. As illustrated in Figure 1A, the dots and filaments often appeared interconnected, suggesting that the filaments were emanating from the dots, which is consistent with the recent findings by Huang et al.[19] Confocal image stacks through VWF-labeled HUVECs revealed that the VWF dots formed clusters in cell subareas where WPBs were also clustered (Figure 1B).

To understand the formation of the VWF dots in greater detail, we designed a series of experiments in which live HUVECs were labeled for VWF during secretagogue stimulation by adding anti-VWF antibodies to the incubation medium. We found serendipitously that the anti-VWF antibodies suppressed the formation of VWF filaments because only VWF dots could be detected in the presence of the antibodies (Figure 1C). The dots developed exclusively on cells that were challenged with secretagogues (PMA, thrombin, or isoproterenol/IBMX) and were never observed on control cells incubated without secretagogues (supplemental Figure 1B-C). The inhibition of VWF-filament formation could be induced by 2 different types of anti-VWF antibodies, could not be mimicked by secondary antibodies (supplemental Figure 1D), and gradually disappeared with increasing dilutions of the VWF antibodies (supplemental Figure 1E). The VWF dots labeled on the surface of live cells also displayed clustering with WPBs, as determined by the labeling with a second species of anti-VWF antibodies after fixation and permeabilization of the cells to allow for detection of VWF inside the cells (Figure 1C). This double VWF-labeling procedure revealed that not all VWF dots were accessible to the surface labeling antibodies. Furthermore, dots were regularly observed that were only partially accessible to the

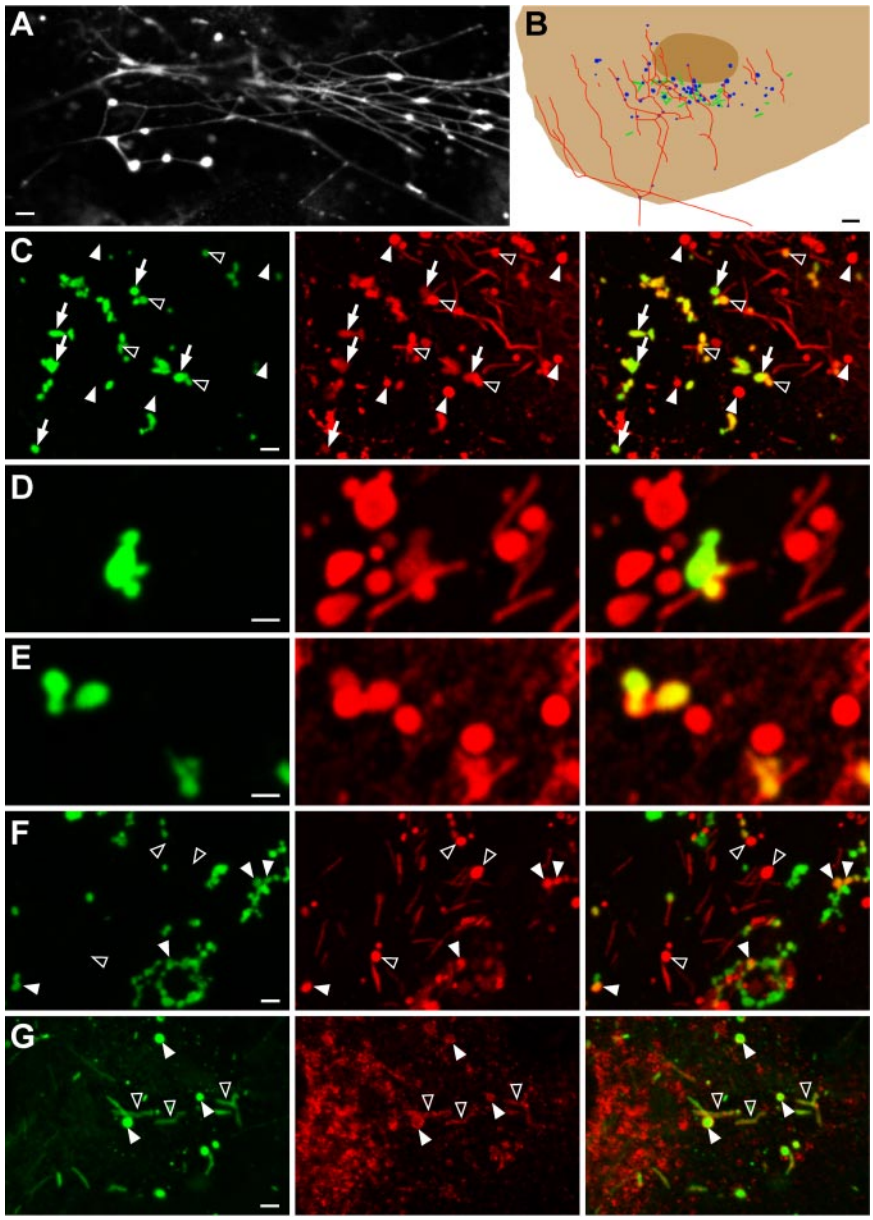

Figure 1. Intra- and extracellular VWF dots in PMA-stimulated endothelial cells. Human umbilical vein endothelial cells (HUVECs) were secretagogue-challenged for 20 minutes with 80nM phorbol 12-myristate 13-acetate (PMA). (A) Immunolabeling of extracellular von Willebrand Factor (VWF; cells were fixed but not permeabilized) shows VWF dots and VWF strings. The dots, which tend to cluster, appear to give rise to the strings. Scale bar is 2 μm. (B) Schematic drawing of part of a HUVEC labeled postfixation and postpermeabilization for VWF. The elongated Weible-Palade bodies (WPBs; green) that have not been exocytosed during the 20 minutes of stimulation are present in the same area as the VWF dots (blue). Most filaments (red) emanate from the same area as well. Scale bar represents 3 μm. (C) Anti-VWF antibodies present during secretagogue challenge prevented formation of VWF strings but not of VWF dots (green channel, left panel). Following fixation and permeabilization, a second VWF antibody (red channel, middle panel) used to label intracellular VWF revealed additional VWF dots that were not labeled with the extracellular anti-VWF antibodies. The right panel depicts the overlay of the green and red channels. Closed arrowheads indicate VWF dots that were not accessible to the extracellular anti-VWF antibodies, open arrowheads indicate partially accessible VWF dots, and arrows indicate fully accessible VWF dots. Scale bar is 2 μm. (D-E) Close-ups of VWF dots labeled extra- or intracellularly (green and red channels, respectively), showing clusters of dots with WPBs. Note that some VWF dots were only partially accessible to the extracellular label. Scale bar is 1 μm. (F) Double-labeling with anti-VWF antibodies during secretagogue challenge (green channel, left panel) and antipropeptide antibodies after fixation and permeabilization (red channel, middle panel). Some VWF dots were also immunoreactive for the propeptide (closed arrowheads), while not all propeptide dots were accessible to the extracellular VWF antibodies (open arrowheads). Scale bar is 2 μm. (G) Double-labeling with anti-VWF (green channel, left panel) and anti-CD63 (red channel, middle panel) antibodies. CD63 labeled WPBs (open arrowheads) and VWF dots (closed arrowheads). Scale bar is 2 μm. All images were acquired with a Leica SL confocal laser-scanning microscope, using a 63× oil-immersion objective with a numeric aperture of 1.40 (Leica HCX PL APO). Fluorochromes used were FITC (conjugated to sheep anti-VWF antibodies; green channel) and Alexa Fluor 568 (conjugated to secondary goat anti–rabbit or goat anti–mouse antibodies; red channel). Minor adjustments of dynamic range (linear adjustments only) were carried out in Adobe Photoshop.

surface labeling antibodies (Figure 1C-E). It thus appeared that the VWF dots on the cell surface originated from intracellular counterparts formed before the release of VWF. In agreement with this hypothesis was the finding that a subpopulation of the VWF dots that were accessible to extracellular VWF antibodies, colocalized with an antipropeptide antibody label applied after cell permeabilization (Figure 1F). Given that the VWF propeptide dissipates very rapidly after being released,[16] it appeared that the propeptide-positive VWF dots represented still partially enclosed cellular compartments.

The intracellular VWF dots showed considerable variation in diameter, ranging from 0.5 to 3 μm. In 3-dimensional renderings of confocal image stacks they had the appearance of blobs, indicating that they corresponded to spherical structures rather than flat sheets (data not shown). Antibodies against the membrane tetraspanin CD63, a marker of mature WPBs,[4,20] lysosomes, and late endosomes, labeled the boundaries of the VWF dots (Figure 1G) whereas antibodies against the membrane tetraspanin Lamp-1, a marker of lysosomes and late endosomes but not WPBs,[21] did not detectably label the dots (data not shown). This suggested that the VWF dots were derived from mature WPBs. Although the smaller dots might have resulted from the rounding up of single WPBs, as has been shown to occur at the onset of lingering kiss–type exocytosis, dots with diameters of 1 μm and above could not be reconciled with such rounding; for instance, the membrane surface area of a sphere with a diameter of 2 μm corresponds roughly to that of 14 WPBs with typical dimensions of 0.15 by 2 μm. To quantify the occurrence and size of these large intracellular VWF dots, we analyzed 63 HUVECs displaying exocytotic activity as determined by the presence of surface-labeled VWF dots. Per cell between 1 and 16 (mean 5.3 ± 3.5) intracellular VWF dots were detected with diameters of 1 μm or above (mean 1.3 ± 0.3 μm). Because VWF dots in this size range were never observed in control cells, the only plausible explanation for their development in secretagogue-challenged cells appeared to be that they resulted from the coalescence of WPBs prior to or during exocytosis. This in turn suggested a focal release mechanism for VWF.

To corroborate the data suggesting focal release of VWF and to gain information on the time course of focal events, we performed

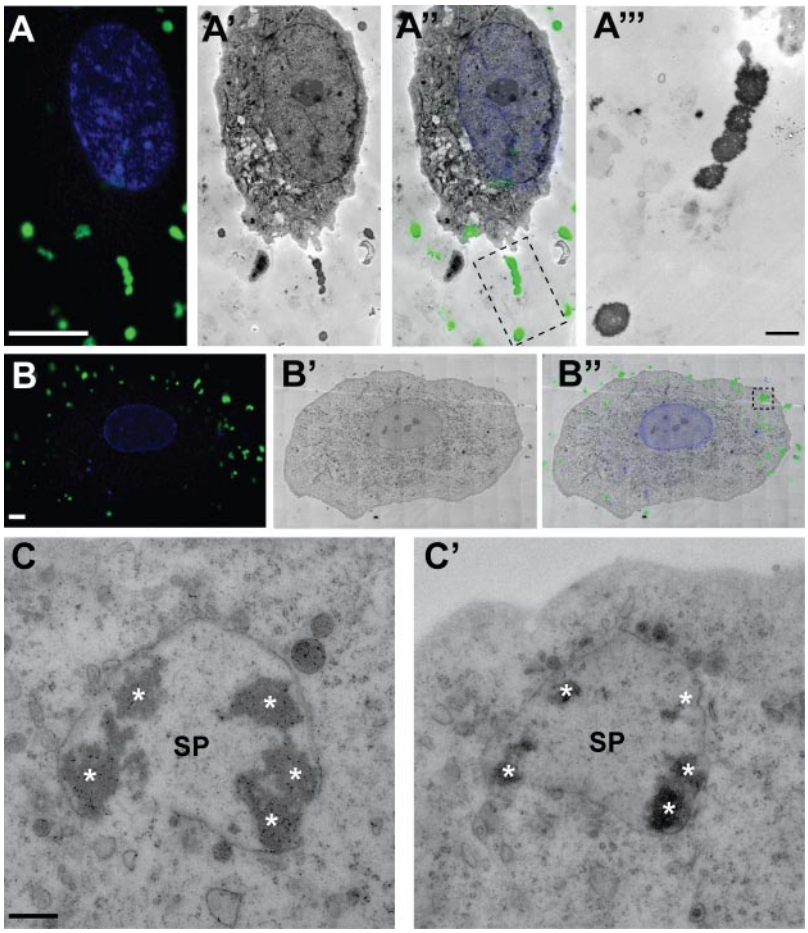

Figure 2. Correlative fluorescence and transmission electron microscopy of VWF dots. HUVECs were stimulated for 20 minutes with 80nM PMA in the presence of FITC-conjugated anti-VWF antibodies to detect extracellularly accessible VWF. (A-A‴) Examples of VWF dots correlated with electron-dense, round-shaped structures outside the cell. (A) Fluorescence micrograph of a HUVEC showing VWF immunofluorescence in green and DAPI in blue. Scale bar represents 10 μm. (A′) Electron micrograph of the cell shown in panel A. (A″) Overlay of the immunofluorescence and electron microscopic images shown in panels A and A′. (A‴) Higher magnification TEM view of the VWF dots in the boxed area in A″. Scale bar represents 1 μm. (B-B″) Example of a cluster of VWF dots correlated with electron-dense, round-shaped structures inside the cell. (B) Fluorescence micrograph of a HUVEC showing VWF immunofluorescence in green and DAPI in blue. Scale bar represents 10 μm. (B′) Electron micrograph of the cell shown in panel B. (B″) Overlay of the immunofluorescence and electron microscopic images shown in panels B and B′. (C-C′) Electron micrographs of 2 consecutive sections corresponding to the boxed area in panel B″, revealing that the cluster of electron-dense VWF dots (asterisks) is contained within a vesicular structure (secretory pod, SP). Scale bar represents 500 nm. Fluorescence images were acquired with a Leica TCS SP5 confocal laser-scanning microscope and a 63× oil-immersion objective with a numeric aperture of 1.4 (Leica HCX Plan APO). Electron micrographs were acquired with an FEI Tecnai 12 TEM at 120 kV and using an FEI Eagle 4kx4k CCD camera.

live-cell imaging experiments in which HUVECs were PMA-stimulated in the presence of FITC-conjugated anti-VWF antibodies. Exocytotic events were detected by the appearance of fluorescent VWF dots. A representative time-lapse movie is available as supplemental Video 1, and a selection of corresponding still images is shown in supplemental Figure 2. After an initial short phase (lasting 20-40 seconds) during which the fluorescent signal expanded and reached plateau, the VWF dots remained stationary for the whole duration of the recordings (up to 25 minutes). However, VWF dots periodically displayed a sudden increase in size, consistent with the focal release of VWF (supplemental Figure 2).

Further characterization of the VWF dots required higher resolution imaging techniques. To identify the ultrastructural equivalents of the VWF dots, we employed 2 correlative light and electron microscopy (CLEM) procedures. The VWF dots were localized using the live-cell extracellular labeling method, thereby allowing us to detect not only dots that corresponded to fully released VWF but also dots that were still partially enclosed. Using the first CLEM approach, which combined confocal laser-scanning microscopy (CLSM) and TEM, we found at the ultrastructural level distinct electron-dense, round-shaped structures that correlated with the fluorescent VWF dots (Figure 2). Due to the inherent discrepancy between the optical section thickness (~ 500 nm) and the ultrathin section thickness (~ 70 nm) it often appeared that these structures were physically separated from the cells (Figure 2A-B). However, as will be demonstrated in the next paragraph, the second CLEM approach combining CLSM and SEM showed that the fluorescent VWF dots correlated with globular structures that always protruded from an underlying plasma membrane. In a number of instances, the VWF structures correlated at the TEM level were enclosed by typically large, membrane-delimited vesicular structures (Figure 2C). These vesicular structures ranged in diameter from 0.5 to 3 μm and enclosed multiple clumps of electron-dense material.

As mentioned in the previous paragraph, correlative CLSM and SEM revealed that the VWF dots corresponded to globular structures on the cell surface, a typical example of which is shown in Figure 3A. Clusters of these globular structures seemed to be connected by short filaments (Figure 3B). Areas on the cell surface that contained VWF dots also displayed round- to oval-shaped pores ranging between 0.8 and 2.1 μm in diameter (mean 1.5 ± 0.4 μm, n = 26; Figure 3C). These pores were considerably larger than the 300- to 800-nm pore-like structures Goerge et al[22] observed in hypoxic HUVECs using atomic force microscopy. On occasion, when the anti-VWF antibodies were omitted from the stimulation medium, VWF strings and associated globular material were captured while in the process of exiting such pores (Figure 3D-E). Incidentally, scanning electron micrographs of VWF strings on secretagogue-challenged HUVECs clearly showed that the VWF strings were formed of multiple filaments bundled together (Figure 3F). The degree of bundling varied, as indicated by the wide range in diameters of VWF strings we measured (14-70 nm, corrected for the thickness of the gold-paladium coat).

The CLEM procedures embodied an inherent trade-off between immunofluorescent signal retention on the one hand, and ultrastructural preservation on the other hand. Therefore, to gain insight in the origin and fate of the large vesicular structures, we pursued their characterization in HUVECs that were processed directly for

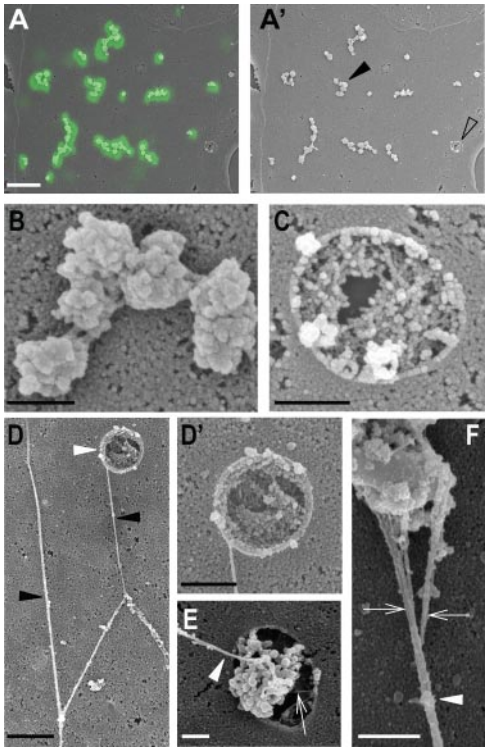

Figure 3. Correlative fluorescence and scanning electron microscopy of VWF dots. HUVECs were stimulated for 20 minutes with 80nM PMA in the presence of FITC-conjugated anti-VWF antibodies to detect extracellularly accessible VWF. (A-A′) Overlay of a correlated VWF fluorescence and scanning electron microscopy (SEM) micrograph of part of a HUVEC, revealing that the VWF immunofluorescence (in green) corresponds to globular structures on the cell surface. Scale bar represents 5 μm. (A′) SEM micrograph of the same area shown in panel A. Cell surface areas containing clusters of VWF dots often contained one or more pores (open arrowhead). (B) Higher magnification of a cluster of VWF dots indicated by the black arrowhead in panel A′. Scale bar represents 500 nm. (C) Higher magnification of the pore indicated by the open arrowhead in panel A′. Notice the clearly defined rim of the pore. Scale bar represents 500 nm. (D-D') When anti-VWF antibodies are omitted during secretagogue challenge, long VWF strings are found on the surface of the cells. (D) Typical example of branching VWF strings (black arrowheads) forming a network. Note the pore (white arrowhead) from which a VWF string emanates. Scale bar represents 1 μm. (D′) Close-up of the secretion pore shown in panel D. Scale bar represents 500 nm. (E) Close-up of another secretion pore releasing globular material and a VWF string (white arrowhead). Pore in the membrane showing globular material and a filament (white arrowhead). The filament appears to arise from the globule. Small filamentous material is also present in the pore (arrow). Scale bar represents 500 nm. (F) High magnification view of a VWF string and associated globule. The string (arrowhead) consists of several entwined filaments (arrows) forming a bundle. Scale bar represents 500 nm. The fluorescence micrograph was acquired using a Leica SP2 confocal laser-scanning microscope and a 63× oil-immersion objective with a numeric aperture of 1.33 (Leica PL APO). Scanning electron micrographs were made with a JEOL JSM-6700F field emission scanning electron microscope at 5.0 kV.

TEM. Because of their prominent size and given that they were only present in secretagogue-challenged HUVECs, the vesicular structures were readily identified. They displayed 3 characteristic features in electron micrographs of ultrathin sections: (1) they contained a core of lacy material, (2) their delimiting membrane showed signs of clathrin-mediated membrane retrieval by the presence of clathrin-coated pits, and (3) they were tightly associated with WPBs (Figure 4). On the basis of these characteristics and because of the involvement of the vesicular structures in regulated exocytosis, we tentatively named them secretory pods.

Fusion of WPBs with secretory pods

The tight association of WPBs with the secretory pods suggested that the WPBs were tethered or docked to them and consequently that the WPBs were in the process of fusing with them. Evidence for this was found in electron tomograms of 150-nm thick plastic sections. Thus Figure 5A shows a digital slice through an electron tomogram in which a WPB has clearly fused with an intracellular secretory pod (a 3-dimensional rendering is shown in Figure 5B, and the full tomogram is available online as supplemental Video 2). The fusing WPBs displayed a number of typical features: (1) they rounded up, (2) their tubular matrix was looser and less electron dense than their nonfused counterparts, and (3) they possessed an electron lucent area interposed between the delimiting membrane and the tubular matrix. The latter 2 features could be explained by the rounding up of the WPB, as the transition of a cylinder to a sphere leads to an increase in volume.

Electron tomography was not only instrumental in unveiling fusion events; it also enabled us to detect tiny vesicles, measuring 30 to 40 nm and which we termed nanovesicles, that were associated with WPBs and secretory pods. Strikingly, we noticed several instances where WPBs connected to secretory pods via nanovesicles, an example of which is shown in Figures 5C and D (full tomograms available online as supplemental Videos 3 and 4). In addition to that, and even more strikingly, the membrane of the nanovesicles sometimes appeared to be continuous with the membrane of the WPBs and secretory pods. This is illustrated in Figure 5E and the corresponding model in Figure 5F. The origin of the nanovesicles could not be determined in this study, but they

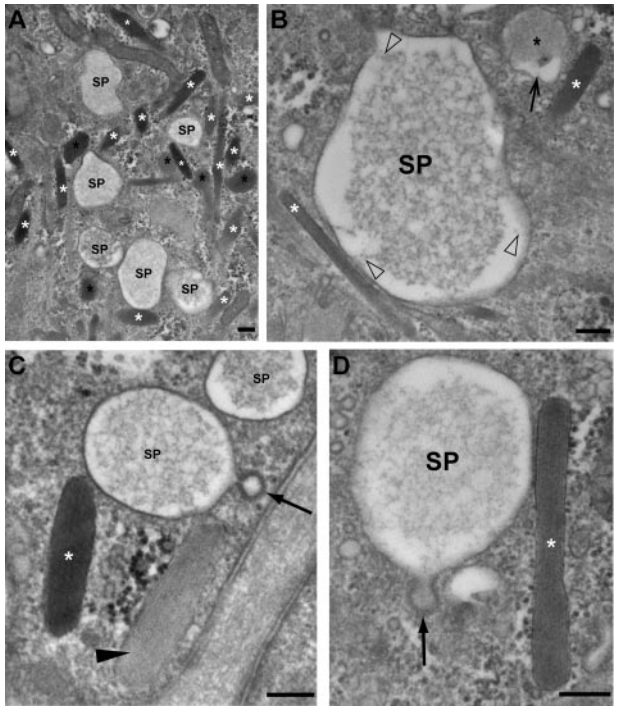

Figure 4. Morphologic characterization of secretory pods visualized by TEM. (A) Low magnification view showing a cluster of SPs and WPBs (white asterisks). Some WPBs have rounded up (black asterisks). (B) An SP displaying a core of lacy material that is connected to the delimiting membrane of the SP by short filaments (open arrowheads). A WPB (white asterisk) makes contact with the SP (bottom left). A rounded WPB (black asterisk) displays an electron lucent area interposed between the delimiting membrane and the matrix (small arrow). (C) A clathrin-coated vesicle (small arrow) is connected to the secretory pod (SP) by a small neck. Note that the WPB labeled with the white asterisk has a denser content than the WPB indicated with an arrowhead. (D) Another example of an SP displaying signs of membrane retrieval (clathrin-coated pit, arrow) and in close contact with a WPB (white asterisk). Note that the membrane of the WPB is electron denser at the interface with the SP, while the delimiting membrane of the SP appears "zippered up" to the WPB. Scale bars represent 100 nm. Images were acquired with an FEI Tecnai 12 TEM at 120 kV and using an FEI Eagle 4kx4k CCD camera.

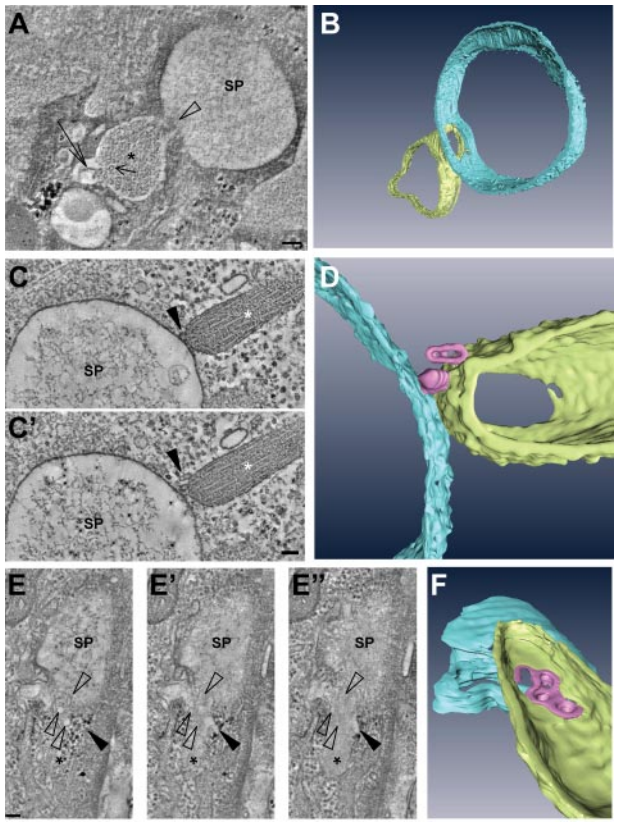

Figure 5. Fusion of WPBs with secretory pods revealed by electron tomography. (A) Digital slice through an electron tomogram of a WPB (asterisk) fusing with an SP. Note the presence of VWF tubules (short arrow), one of which appears to unfurl (long arrow). (B) Three-dimensional model of the tomogram shown in panel A. (C-D) Example of an SP making contact with a WPB via nanovesicles. (C,C′) Two digital slices through a tomogram showing the nanovesicles (arrowhead) intercalated between the WPB (asterisk) and SP. (D) Three-dimensional model of the tomogram shown in panels C and C′. (E-F) Nanovesicles fusing with a WPB and SP. (E-E″) Series of digital slices through a tomogram of a WPB (asterisk) in the process of fusing with an SP. Open arrowheads indicate nanovesicles whereas the black arrowhead points toward an electron lucent area interposed between the WPB delimiting membrane and the tubular matrix. (F) Three-dimensional model of the tomogram shown in panels E to E″. Scale bars represent 100 nm. Tilt series for tomographic reconstruction were acquired with an FEI Tecnai 12 TEM at 120 kV and using an FEI Eagle 4kx4k CCD camera.

were clearly related to secretory activity, since we rarely found them in the vicinity of WPBs in electron tomograms taken from control HUVECs. Thus in 12 tomograms of secretory pods we counted per tomogram between 6 and 32 nanovesicles (mean 13.3 ± 8.3) surrounding the pods (20 in total) and associated WPBs (112 in total), whereas in 9 tomograms of WPBs (19 in total) in control cells, we only found 4 nanovesicles (0.4 ± 0.7). Taken together, these data suggested that WPBs fused with the secretory pods by intermediate of nanovesicles.

Secretory pods are release sites for VWF

The immunofluorescence, live-cell imaging, and CLEM data indicated that a subpopulation of secretory pods connects to the extracellular space. Further evidence for this was obtained from experiments using colloidal lanthanum as an electron-dense extracellular tracer. By means of control, we verified that the lanthanum stain produced characteristic opaque precipitates on the endothelial cell surface, in caveolae, and in intercellular spaces (data not shown). Lanthanum precipitates were also found in 78% of the secretory pods analyzed (n = 113). Interestingly, the lanthanum associated preferentially with the lacy material present in the lumen of the secretory pods (Figure 6A). In addition, we found several examples of secretory pods that formed small protrusions filled with the lanthanum stain. In the example shown in Figure 6B, the protrusion seems to connect with a WPB.

To determine the nature of the secretory pod connections to the extracellular space, we traced secretory pods by serial-sectioning TEM. Several secretory pods that were analyzed in this manner opened up into the apical plasma membrane via a large pore of around 1 μm in size (Figure 6C). When the cells had been secretagogue challenged in the presence of anti-VWF antibodies, the pores were covered by the typical electron-dense spherules of VWF protruding into the extracellular space (Figure 6D-F, and supplemental Video 5).

Secretory pod formation is not exclusive for PMA

Phorbol esters including PMA are widely used as potent stimulators of regulated exocytosis. Being stable analogs of the signaling lipid, diacylglycerol (DAG), they were initially thought to activate specifically protein kinase C, which mediates phosphorylation of several exocytotic proteins.[23] In more recent years, however, receptors for DAG/phorbol esters have been identified on other proteins, such as the secretory vesicle priming protein, Munc13.[24,25] Therefore, one could argue that secretory-pod formation is a PMA-specific effect resulting from potent stimulation outside the physiologic range. To test this, we also investigated secretory pod formation following stimulation with thrombin, which is considered a more physiologic secretagogue. As shown in Figure 7A and B, thrombin appeared as potent as PMA in inducing secretory pods. In 37 cells displaying exocytotic activity, we counted per cell between 1 and 14 (mean 4.2 ± 3.0) intracellular VWF dots with diameters of 1 μm or above (mean 1.4 ± 0.4 μm). These values were very close to those determined for PMA. Likewise, in the absence of extracellular VWF antibodies, thrombin stimulation induced VWF dots and strings indistinguishable from PMA stimulation (Figure 7C). Electron microscopy further confirmed that thrombin challenge led to secretory pod formation (Figure 7D).

Discussion

The pre- and postfixation/permeabilization VWF labeling strategy made it possible to distinguish sites of fully released VWF from large spherical VWF compartments, which we termed secretory pods. Not all secretory pods were accessible to extracellular anti-VWF antibodies or lanthanum, indicating that they can form prior to fusion with the plasma membrane. The colocalization of CD63 with the secretory pods suggested that they originated from mature WPBs. However, given the diameter of the intracellular secretory pods, measuring up to 3 μm, they could not be attributed to the rounding up of single WPBs. Instead, they appeared to result from the coalescence of multiple WPBs prior to exocytosis, as was suggested by the finding that secretory pods tend to cluster with WPBs, and confirmed by the electron tomograms of WPBs fusing with secretory pods. Exocytosis of aggregates formed by the prior homotypic fusion of secretory granules has been referred to as multigranular exocytosis and is related to compound exocytosis, although in the latter, secretory granules exocytose individually and sequentially (for review, see Pickett and Edwardson[26]). The stepwise increases in diameter of exocytosed VWF dots monitored by live-cell imaging are in agreement with a focal release

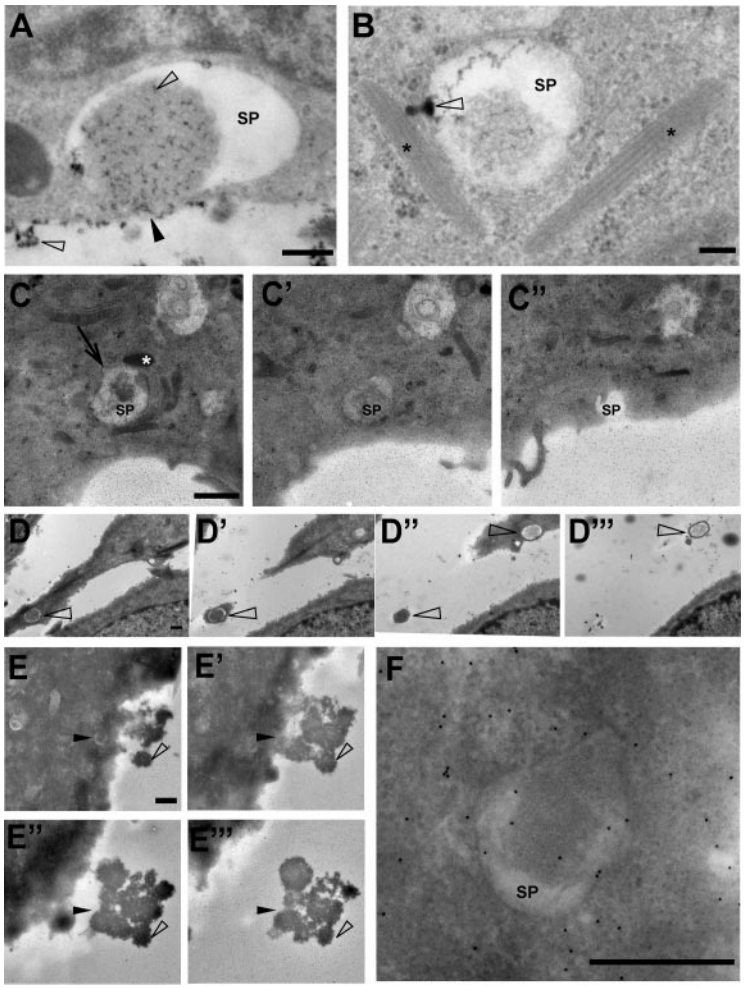

Figure 6. Secretory pods can connect to the extracellular space. (A-B) Lanthanum was used as a tracer of extracellular spaces. Precipitates of lanthanum, which are present as opaque speckles (open arrowheads), have mixed with the content of the SP shown in this example. The SP appears to have fused with the plasmamembrane (black arrowhead). Scale bar represents 100 nm. (B) The SP in this example shows a funnel-shaped protrusion (open arrowhead) that is filled with lanthanum precipitate and connects to a WPB close by (WPBs are indicated with asterisks). The funnel-shaped structure may correspond to fused nanovesicles. Scale bar represents 100 nm. (C,C′,C″) Consecutive sections of 150-nm thickness, through an SP that in panel C″ opens up into the extracellular space via an omega-shaped figure. The SP is in contact with a WPB (white asterisk in panel C) and displays a clathrin-coated pit (arrow in C). Scale bar represents 1 μm. (D-D‴) Consecutive sections through
2 SPs (open arrowheads). In panel D‴, the SP at the top is surrounded by only a small rim of the cell surface, suggesting that the plasma membrane forms an elevation around the exit site, that is, secretion pore, of the SP. Scale bar represents 500 nm. (E,E′,E″,E‴) Consecutive sections through a secretory pod (black arrowhead in panel E) in a HUVEC that was secretagogue-challenged in the presence of anti-VWF antibodies to generate electron-dense globules of VWF (open arrowhead). The position of the SP in panel E is indicated in the consecutive sections E′ through E‴. Note that the VWF globules emanate from the SP. Scale bar represents 1 μm. (F) Enlargement of the SP shown in panel E. Scale bar represents 500 nm. (C-C″,E-F) The small speckles in panels C to C″ and panels E and F represent gold particles used as fiducial markers for electron tomography. Electron micrographs and tilt series were acquired with an FEI Tecnai 12 TEM at 120 kV and using an FEI Eagle 4kx4k CCD camera.

mechanism for VWF, and may result from remodeling of underlying secretory pods or fusion of WPBs with secretory pods that already underwent exocytosis.

Previously, we have shown that WPBs in nonstimulated cells can adopt strikingly irregular shapes, likely as a result of homotypic fusion between WPBs, suggesting that homotypic fusion provides a mechanism for WPB maturation.[6] The present data extend the role of homotypic fusion to that of secretory pod formation and regulated exocytosis. However, the mechanisms of WPB maturation and secretory pod formation are clearly distinct: while VWF tubules accompanied all stages of WPB maturation, they were absent in secretory pods. Instead, VWF tubules appeared to have disassembled in the secretory pods, giving rise to a mesh of VWF filaments.

The secretory pods were a prominent feature of HUVECs displaying exocytotic activity. On average, cells contained 4 (thrombin) or 5 (PMA) pods with a mean diameter of 1.4 or 1.3 μm, respectively, the surface area of which corresponds to that of 7 or 6 typically sized WPBs per pod. This suggests that in an average cell, at least 28 to 30 WPBs undergo multigranular exocytosis. Because these calculations only take into account secretory pods that have not yet engaged in exocytosis, the actual number of pod-forming WPBs will be higher. Howell et al[27] determined that the average number of WPBs in HUVECs cultured to confluence is around 50. Our own unpublished observations suggest a higher number, ranging between 100 and 200. It follows that the percentage of WPBs participating in secretory pod formation is at least 15% to 30% thereby implying that multigranular exocytosis represents a major pathway for VWF release.

Several studies have previously provided data suggesting compound or multigranular exocytosis events in endothelial cells. Thus Fujimoto[28] described secretory pod-like structures that formed in endothelial cells of toad aorta following secretagogue administration, and Richardson et al[29] demonstrated in rat endothelial cells that these structures contained VWF-immunoreactive material. Lastly, Zupancic et al[30] observed in patch-clamped HUVECs large step increases in membrane capacitance, indicative of fusion events, that were too large to be accounted for by the exocytosis of single WPBs. Despite these studies, multigranular exocytosis does not appear to be generally recognized as a biologically significant mechanism, that is, a major pathway, for VWF release. This may be due in part to the circumstantial nature of the evidence. For instance, direct evidence for fusion between WPBs and secretory pods was hitherto lacking, and likewise it could not be ruled out that organelles unrelated to WPBs contributed to the large step increases in membrane capacitance. A further reason why multigranular exocytosis of VWF may have been unappreciated is that live-cell imaging studies of VWF release using GFP-tagged VWF have thus far only yielded data illustrating exocytosis of single WPBs.[12-16] It is of note, however, that none of the studies showing single WPB exocytosis, including 2 electron microscopy investigations,[31,32] demonstrated VWF strings in association with the single events. By contrast, in the present study, VWF strings visualized by SEM were found to emanate from large pores in

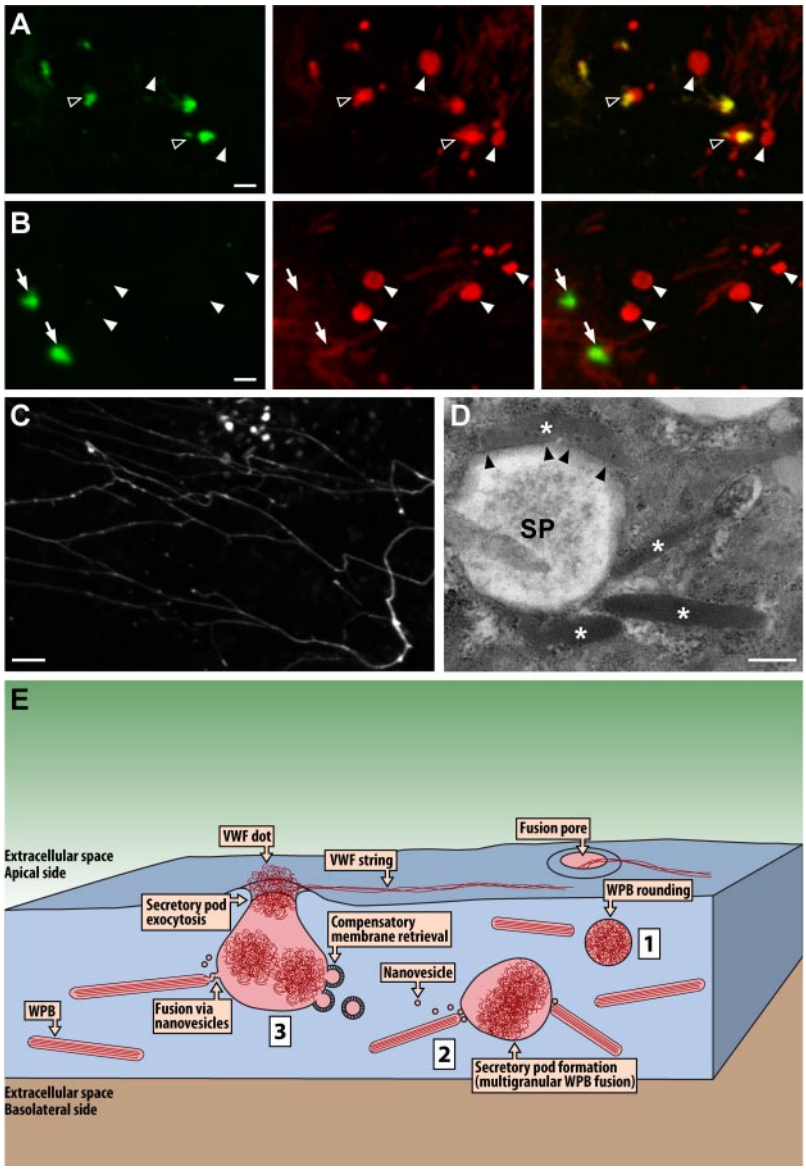

Figure 7. Secretory pod formation induced by thrombin. HUVECs were secretagogue challenged for 10 minutes with thrombin at a concentration of 1 U/mL. (A-B) Examples of VWF dots revealed by labeling with 2 distinct VWF antibodies, the first applied during secretagogue challenge (green channel, left panels) and the second after fixation and permeabilization (red channel, middle panels). The right panels depict the overlays of the green and red channels. Closed arrowheads indicate VWF dots that were not accessible to the extracellular anti-VWF antibodies (ie, nonfused SPs), open arrowheads indicate partially accessible VWF dots (ie, fused SPs), and arrows indicate fully accessible VWF dots. Scale bar is 2 μm. (C) Example of VWF strings and VWF dots induced by thrombin stimulation in the absence of VWF antibodies. VWF labeling was performed only after fixation and permeabilization. Scale bar represents 5 μm. Microscopy and fluorochromes used were as described in Figure 1 legend. (D) Electron micrograph of a thrombin-induced SP. Asterisks indicate WPBs clustering around or making close contact with the pod. Notice in particular the top WPB that appears to be docking lengthwise onto the pod (arrowheads). Scale bar represents 0.5 μm. Microscopy was as described in Figure 2 legend. (E) Hypothetical model summarizing the data presented herein. Secretagogue challenge of HUVECs induces multigranular exocytosis of WPBs. The initial event leading to this process may be WPB rounding (1), although WPB rounding has also been implicated in lingering-kiss exocytosis. Coalescence of WPBs is mediated by nanovesicles and leads to the formation of intracellular secretory pods (2). Subsequent fusion of the secretory pods with the plasma membrane results in secretory pod exocytosis (3). VWF is released via the fusion pore of the SPs. The delimiting membrane of the SPs is reinternalized via clathrin-mediated compensatory membrane retrieval. WPBs may continue to fuse with multigranular aggregates that have already undergone exocytosis.

the endothelial cell membrane, and by TEM such pores were connected to secretory pods, indicating that multigranular exocytosis can give rise to VWF strings.

The detection of clathrin-coated pits on the secretory pods raises the question as to the extent to which the cell and secretory pod membranes mix after their fusion. If membrane mixing is limited, which is implied by the clathrin recruitment to the pod membrane, then it is likely that multigranular exocytosis favors the release of WPB core proteins, of which VWF and its propeptide constitute the bulk, and that the major membrane proteins CD63 and P-selectin are retained, that is, internalized. Although the role of CD63 remains to be elucidated, it has been proposed that it is involved in mediating early inflammatory responses in endothelial cells.[4] Likewise, the function of the leukocyte receptor P-selectin is to induce leukocyte rolling on endothelial cells during an inflammatory reaction.[33] It is thus conceivable that multigranular exocytosis allows for the differential release of WPB constituents, favoring the secretion of hemostasis factors and the retention of inflammatory mediators. Interestingly, Cleator et al[34] measured differential release profiles of P-selectin and VWF, which they attributed to the existence of subpopulations of WPBs with different compositions and susceptibilities to secretagogues. Besides the aforementioned paper, there are more studies exposing the heterogeneous nature of WPBs.[17,35] But there is also additional evidence for the differential release of WPB constituents during exocytosis. Thus, as mentioned in the Introduction, Babich et al[14] have shown that a subset of WPBs engages in a slow form of kiss-and-run exocytosis (lingering kiss) whereby a 10- to 12-nm fusion pore forms and acts as a molecular sieve, allowing the smaller proteins, interleukin-8 and CD63, to be released while the larger proteins, VWF, Propeptide, and P-selectin, are retained. Altogether a picture emerges where the secretion of WPB cargo is modulated at the level of both WPB biogenesis/maturation and exocytotic release mode.

Huang et al[9] recently recreated in vitro the formation of VWF tubules, and were thus able to estimate that a tubule of 1 μm long might correspond to an unfurled filament of 47 μm long. We have shown previously that a WPB can contain close to 60 tubules and that their majority spans the entire WPB length.[6] Together, these data would imply that a typical WPB of 2 μm long could give rise to more than 5 mm of VWF filament provided that the VWF multimers can self-assemble into longer multimers, for which evidence has been described.[36,37] However, the thicknesses of

ultralong VWF strings (14-70 nm) we measured in SEM images were a multiple of that of an unfurled VWF tubule (~ 7 nm, presuming it to correspond to the tubule wall thickness),[9] suggesting that the VWF strings have a higher degree of compaction than a single unfurled filament. Furthermore, as demonstrated by our SEM data and in agreement with Huang et al,[19] the VWF strings are composed of branching bundles of multiple VWF filaments. It therefore appears unlikely that the VWF content of a single WPB is sufficient to account for an entire branching bundle of ultralong VWF filaments. In this line of reasoning, multigranular exocytosis via secretory pods would allow for the pooling of VWF from multiple WPBs.

Intriguingly, the fusion of WPBs with secretory pods appeared to occur via interposing vesicles, which we termed nanovesicles due to their remarkably small size. Somewhat larger (50- to 70-nm) but still small cytoplasmic vesicles have been similarly implicated in the multigranular exocytosis by basophilic leukocytes.[38] Therefore, granule-to-granule fusion by intermediate of small vesicles may represent a common mechanism that is not restricted to vascular endothelial cells. Moreover, in parotid acinar cells it has been shown by membrane capacitance measurements that the exocytosis of zymogen granules is preceded by an exocytotic phase that cannot be resolved as individual fusion events, suggesting that this phase corresponds to the fusion of small vesicles.[39] In agreement with these findings, a model has been proposed in which a minor regulated secretory pathway of small, rapidly fusing vesicles enables the subsequent exocytosis of zymogen granules by providing fusion sites.[40] Further studies will be required to investigate the precise nature of the nanovesicles and their functional relevance.

By way of conclusion, we propose a model summarizing and integrating the data presented here (Figure 7E). Evidence is provided that multigranular exocytosis constitutes an important pathway for the regulated release of VWF by vascular endothelial cells. A novel structure, which we termed secretory pod, was identified in the multigranular exocytotic pathway. Secretory pod formation resulted from the coalescence of WPBs prior to exocytosis and this process was mediated by nanovesicles. Endothelial-cell multigranular exocytosis may facilitate the formation of VWF strings.

Acknowledgments

The authors thank Erik Bos and Karen A. Jansen for expert technical assistance, Jos J. M. Onderwater, Ronald Limpens, and Joke van der Meer for help with the SEM, Kèvin Knoops for help with Amira, and Prof A. K. Raap and Prof H. J. Tanke for critically reading the manuscript. Mouse monoclonal antibodies CLB-Pro-14.3 against the propeptide of VWF were a generous gift from Dr J. Voorberg, Sanquin, Amsterdam.

This research was supported in part by the Dutch Organization for Scientific Research (NWO TOP-grant 91209006).

Authorship

Contribution: K.M.V. and J.A.V. designed and performed research, analyzed and interpreted the data, and wrote the paper; L.F.v.D., M.J.M., G.-J.H., and T.J.A. performed research; and A.J.K. provided experimental design and manuscript review.

Conflict-of-interest disclosure: The authors declare no competing financial interests.

Correspondence: Jack A. Valentijn, Department of Molecular Cell Biology, Leiden University Medical Center, P O Box 9600, 2300 RC Leiden, The Netherlands; e-mail: j.a.valentijn@lumc.nl.

References

1. Wagner DD, Frenette PS. The vessel wall and its interactions. *Blood.* 2008;111(11):5271-5281.
2. Weibel ER, Palade GE. New cytoplasmic components in arterial endothelia. *J Cell Biol.* 1964;23: 101-112.
3. Groot E, de Groot PG, Fijnheer R, Lenting PJ. The presence of active von Willebrand factor under various pathological conditions. *Curr Opin Hematol.* 2007;14(3):284-289.
4. Metcalf DJ, Nightingale TD, Zenner HL, Lui-Roberts WW, Cutler DF. Formation and function of Weibel-Palade bodies. *J Cell Sci.* 2008; 121(Pt 1):19-27.
5. Kumar RA, Moake JL, Nolasco L, et al. Enhanced platelet adhesion and aggregation by endothelial cell-derived unusually large multimers of von Willebrand factor. *Biorheology.* 2006;43(5):681-691.
6. Valentijn KM, Valentijn JA, Jansen KA, Koster AJ. A new look at Weibel-Palade body structure in endothelial cells using electron tomography. *J Struct Biol.* 2008;161(3):447-458.
7. Zenner HL, Collinson LM, Michaux G, Cutler DF. High-pressure freezing provides insights into Weibel-Palade body biogenesis. *J Cell Sci.* 2007; 120(Pt 12):2117-2125.
8. Berriman JA, Li S, Hewlett LJ, et al. Structural organization of Weibel-Palade bodies revealed by cryo-EM of vitrified endothelial cells. *Proc Natl Acad Sci U S A.* 2009;106(41):17407-17412.
9. Huang RH, Wang Y, Roth R, et al. Assembly of Weibel-Palade body-like tubules from N-terminal domains of von Willebrand factor. *Proc Natl Acad Sci U S A.* 2008;105(2):482-487.
10. Michaux G, Cutler DF. How to roll an endothelial cigar: the biogenesis of Weibel-Palade bodies. *Traffic.* 2004;5(2):69-78.
11. Wagner DD. Cell biology of von Willebrand factor. *Annu Rev Cell Biol.* 1990;6:217-246.
12. Romani de Wit T, Rondaij MG, Hordijk PL, Voorberg J, van Mourik JA. Real-time imaging of the dynamics and secretory behavior of Weibel-Palade bodies. *Arterioscler Thromb Vasc Biol.* 2003;23(5):755-761.
13. Babich V, Knipe L, Hewlett L, et al. Differential effect of extracellular acidosis on the release and dispersal of soluble and membrane proteins secreted from the Weibel-Palade body. *J Biol Chem.* 2009;284(18):12459-12468.
14. Babich V, Meli A, Knipe L, et al. Selective release of molecules from Weibel-Palade bodies during a lingering kiss. *Blood.* 2008;111(11):5282-5290.
15. Erent M, Meli A, Moisoi N, et al. Rate, extent and concentration dependence of histamine-evoked Weibel-Palade body exocytosis determined from individual fusion events in human endothelial cells. *J Physiol.* 2007;583(Pt 1):195-212.
16. Hannah MJ, Skehel P, Erent M, et al. Differential kinetics of cell surface loss of von Willebrand factor and its propolypeptide after secretion from Weibel-Palade bodies in living human endothelial cells. *J Biol Chem.* 2005;280(24):22827-22830.
17. Rondaij MG, Bierings R, Kragt A, van Mourik JA, Voorberg J. Dynamics and plasticity of Weibel-Palade bodies in endothelial cells. *Arterioscler Thromb Vasc Biol.* 2006;26(5):1002-1007.
18. Sporn LA, Marder VJ, Wagner DD. Inducible secretion of large, biologically potent von Willebrand factor multimers. *Cell.* 1986;46(2):185-190.
19. Huang J, Roth R, Heuser JE, Sadler JE. Integrin alpha (v) beta(3) on human endothelial cells binds von Willebrand factor strings under fluid shear stress. *Blood.* 2009;113(7):1589-1597.
20. Vischer UM, Wagner DD. CD63 is a component of Weibel-Palade bodies of human endothelial cells. *Blood.* 1993;82(4):1184-1191.
21. Arribas M, Cutler DF. Weibel-Palade body membrane proteins exhibit differential trafficking after exocytosis in endothelial cells. *Traffic.* 2000;1(10): 783-793.
22. Goerge T, Niemeyer A, Rogge P, et al. Secretion pores in human endothelial cells during acute hypoxia. *J Membr Biol.* 2002;187(3):203-211.
23. Morgan A, Burgoyne RD, Barclay JW, et al. Regulation of exocytosis by protein kinase C. *Biochem Soc Trans.* 2005;33(Pt 6):1341-1344.
24. Rhee JS, Betz A, Pyott S, et al. Beta phorbol ester- and diacylglycerol-induced augmentation of transmitter release is mediated by Munc13s and not by PKCs. *Cell.* 2002;108(1):121-133.
25. Silinsky EM, Searl TJ. Phorbol esters and neurotransmitter release: more than just protein kinase C? *Br J Pharmacol.* 2003;138(7):1191-1201.
26. Pickett JA, Edwardson JM. Compound exocytosis: mechanisms and functional significance. *Traffic.* 2006;7(2):109-116.
27. Howell GJ, Herbert SP, Smith JM, et al. Endothelial cell confluence regulates Weibel-Palade body formation. *Mol Membr Biol.* 2004;21(6):413-421.
28. Fujimoto S. Degranulation of endothelial specific granules of the toad aorta after treatment with compound 48/80. *Anat Rec.* 1982;203(2):197-204.

29. Richardson M, Tinlin S, De Reske M, et al. Morphological alterations in endothelial cells associated with the release of von Willebrand factor after thrombin generation in vivo. *Arterioscler Thromb.* 1994;14(6):990-999.

30. Zupancic G, Ogden D, Magnus CJ, Wheeler-Jones C, Carter TD. Differential exocytosis from human endothelial cells evoked by high intracellular Ca(2+) concentration. *J Physiol.* 2002; 544(pt 3):741-755.

31. McNiff JM, Gil J. Secretion of Weibel-Palade bodies observed in extra-alveolar vessels of rabbit lung. *J Appl Physiol.* 1983;54(5):1284-1286.

32. Trillo AA, Prichard RW. Early endothelial changes in experimental primate atherosclerosis. *Lab Invest.* 1979;41(4):294-302.

33. Lowenstein CJ, Morrell CN, Yamakuchi M. Regulation of Weibel-Palade body exocytosis. *Trends Cardiovasc Med.* 2005;15(8):302-308.

34. Cleator JH, Zhu WQ, Vaughan DE, Hamm HE. Differential regulation of endothelial exocytosis of P-selectin and von Willebrand factor by protease-activated receptors and cAMP. *Blood.* 2006; 107(7):2736-2744.

35. Fiedler U, Scharpfenecker M, Koidl S, et al. The Tie-2 ligand angiopoietin-2 is stored in and rapidly released upon stimulation from endothelial cell Weibel-Palade bodies. *Blood.* 2004;103(11): 4150-4156.

36. Barg A, Ossig R, Goerge T, et al. Soluble plasma-derived von Willebrand factor assembles to a haemostatically active filamentous network. *Thromb Haemost.* 2007;97(4):514-526.

37. Savage B, Sixma JJ, Ruggeri ZM. Functional self-association of von Willebrand factor during platelet adhesion under flow. *Proc Natl Acad Sci U S A.* 2002;99(1):425-430.

38. Dvorak AM, Galli SJ, Morgan E, et al. Anaphylactic degranulation of guinea pig basophilic leukocytes. I. Fusion of granule membranes and cytoplasmic vesicles formation and resolution of degranulation sacs. *Lab Invest.* 1981;44(2):174-191.

39. Chen Y, Warner JD, Yule DI, Giovannucci DR. Spatiotemporal analysis of exocytosis in mouse parotid acinar cells. *Am J Physiol Cell Physiol.* 2005;289(5):C1209-1219.

40. Castle AM, Huang AY, Castle JD. The minor regulated pathway, a rapid component of salivary secretion, may provide docking/fusion sites for granule exocytosis at the apical surface of acinar cells. *J Cell Sci.* 2002;115(Pt 14):2963-2973.